Color Tuning of Multi-Resonant Thermally Activated Delayed Fluorescence Emitters Based on Fully Fused Polycyclic Amine/Carbonyl Frameworks

John Marques dos Santos,[a] Chin-Yiu Chan,[c] Shi Tang,[d] David Hall,[a,b] Tomas Matulaitis,[a] David B. Cordes,[a] Alexandra M. Z. Slawin,[a] Youichi Tsuchiya,[c] Ludvig Edman,[d] Chihaya Adachi,[c*] Yoann Olivier,[b*] and Eli Zysman-Colman[a*]*

[a] Organic Semiconductor Centre, EaStCHEM School of Chemistry, University of St Andrews, St Andrews, KY16 9ST, UK. E-mail: eli.zysman-colman@st-andrews.ac.uk;

[b] Laboratory for Computational Modeling of Functional Materials, Namur Institute of Structured Matter, University of Namur, Rue de Bruxelles, 61, 5000 Namur, Belgium. E-mail: yoann.olivier@unamur.be

[c] Center for Organic Photonics and Electronics Research (OPERA), Kyushu University, Motooka 744, Nishi-ku, Fukuoka 819-0395, Japan.

[d] The Organic Photonics and Electronics Group, Department of Physics, Umeå University, SE-90187 Umeå, Sweden

Electronic Supporting Information

Table of content
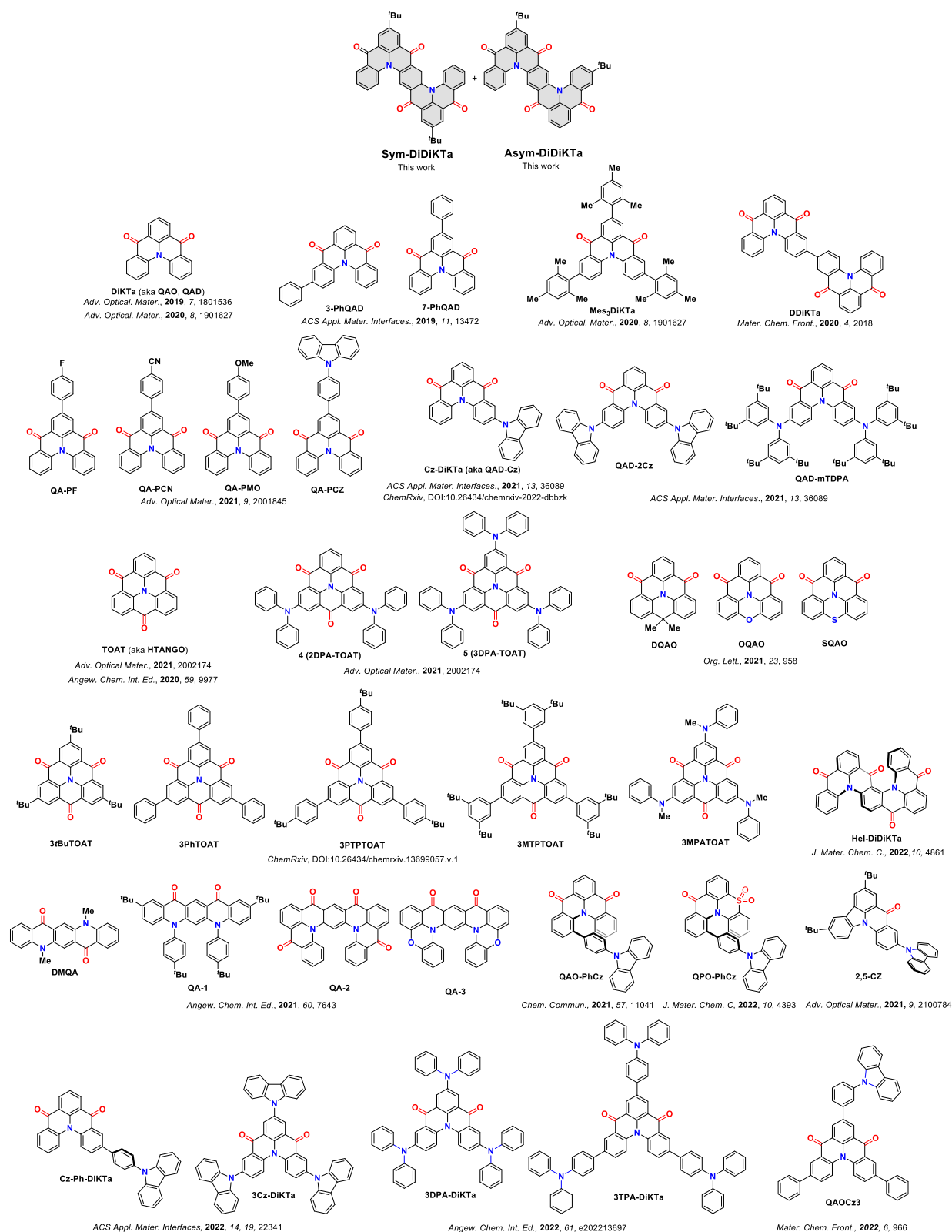
Figure S1. Chemical structures of prior examples of N/Carbonyl MR-TADF emitters.[1–15]

Table S1. Photophysical properties of N-Carbonyl MR-TADF emitters.

Compound	Medium	λ_{PL} / nm	Φ_{PL} / %	τ_D / μs	ΔE_{ST} / eV	Ref
Sym-DiDiKTa	1% in mCP	542	64	1700	0.24[a]	This work
Asym-DiDiKTa	1% in mCP	547	57	2100	0.23[a]	This work
DiKTa/QAO/QAD	5 wt% mCP	466	72	93.3	0.19	1-2
3-PhQAD	2 wt% mCP	478	73	250	0.18	3
7Ph-QAD	2 wt% mCP	472	68	474	0.19	4
Mes₃DiKTa	3.5 wt% mCP	477	80	20	0.21	2
DDiKTa	9 wt% DPEPO	490	72	1.2	0.16	4
QA-PF	3 wt% mCP	478	89	346.9	0.24	5
QA-PCN	3 wt% mCP	477	68	223.9	0.18	5
QA-PMO	3 wt% mCP	485	66	484.1	0.25	5
QA-PCZ	3 wt% mCP	480	71	339.1	0.21	5
Cz-DiKTa/QAD-Cz	1 wt% mCP	500	100	205	0.17	6
QAD-2Cz	12 wt% mCP	526	100	130	0.17	6
QAD-mTDPA	1.5 wt% CBP	587	97	269	0.33	6
DQAO	8 wt% mCP	472	59	111	0.19	7
OQAO	5 wt% CBP	534	90	205	0.16	7
SQAO	1 wt% mCPCN	560	65	78	0.16	7
TCTANGO	Chloroform	445	5	N/A	N/A	8
TBTANGO	Neat film	~554	N/A	N/A	N/A	8
TITANGO	Neat film	~561	N/A	N/A	N/A	8
*t*BuTANGO	Chloroform	440	13	N/A	N/A	8
TOAT/HTANGO	Chloroform	422	1	N/A	0.34	8-9
2DPA-TOAT	3 wt% mCBP	~598	46	3844	0.34	9
3DPA-TOAT	3 wt% mCBP	~590	46	2142	0.34	9
3tBuTOAT	15 wt% SiCz	484	N/A	N/A	0.29	10
3PhTOAT	15 wt% mCP	516	97	N/A	0.12	10
3PTPTOAT	15 wt% mCP	520	93	N/A	0.16	10
3MTPTOAT	15 wt% mCP	502	92	N/A	0.14	10
3MPATOAT	15 wt% CBP	654	N/A	N/A	0.28	10
DMQA	Toluene	~520	78	N/A	N/A	11
QA-1	3 wt% PPCz	457	94	655	0.29	11
QA-2	3 wt% PPCz	465	97	48	0.19	11
QA-3	3 wt% PPCz	523	99	307	0.19	11
Hel-DiDiKTa	1 wt% mCP	477	4.1	5.43	0.13	12
QAO-PhCz	5% wt% in mCP	461[a]	46	40.36	0.11[a]	13
QPO	18% wt% in mCP	431[a]	18	468	0.23	14
QPO-PhCz	18% wt% in DPEPO	446[a]	51	536	0.23	14
Cz-Ph-DiKTa	2 wt% mCP	486	77	155	0.10	15
3Cz-DiKTa	2 wt% mCP	539	78	287	0.16	15
3DPA-DiKTa	2 wt% mCP	617	60	323	0.20	16
3TPA-DiKTa	2 wt% mCP	551	93	131	0.13	16
2,5-Cz	3.5 wt% mCBP	459[a]	81	619	0.29[a]	17
QAOCz3	5 wt% CBP	495	99	26.5	0.16[a]	18

The medium is specified in the second column, unless specified with a superscript as shown below:
[a] toluene
~ Indicates that the data was obtained using a graphical fitting software.

1. Experimental Section

General Synthetic Procedures. All reagents and solvents were obtained from commercial sources and used as received. Air-sensitive reactions were performed under a nitrogen atmosphere using Schlenk techniques, no special precautions were taken to exclude air or moisture during work-up. DCM was obtained from a MBraun SPS5 solvent purification system. Flash column chromatography was carried out using silica gel (Silia-P from Silicycle, 60 Å, 40-63 μm). Analytical thin-layer-chromatography (TLC) was performed with silica plates with aluminum backings (250 μm with F-254 indicator). TLC visualization was accomplished by 254/365 nm UV lamp. HPLC analysis was conducted on a Shimadzu LC-40 HPLC equipped with a GPC using a Shim-pack GPC-803 column with THF as mobile phase. GCMS analysis was conducted using a Shimadzu QP2010SE GC-MS equipped with a Shimadzu SH-Rtx-1 column (30 m × 0.25 mm). ^{1}H and ^{13}C NMR spectra were recorded on a Bruker Advance spectrometer (400 MHz for ^{1}H and either 101 or 126 MHz for ^{13}C). The following abbreviations have been used for multiplicity assignments: "s" for singlet, "d" for doublet, "t" for triplet, "m" for multiplet, and "dd" for doublet of doublets. ^{1}H and ^{13}C NMR spectra were referenced residual solvent peaks with respect to TMS ($\delta = 0$ ppm). Melting points were measured using open-ended capillaries on an Electrothermal 1101D Mel-Temp apparatus and are uncorrected. High-resolution mass spectrometry (HRMS) was performed in the Mass Spectrometry facility at the University of St Andrews.

Electrochemistry Measurements. Cyclic Voltammetry (CV) analysis was performed on an Electrochemical Analyzer potentiostat model 620E from CH Instruments at a sweep rate of 100 mV/s. Differential pulse voltammetry (DPV) was conducted with an increment potential of 0.01 V and a pulse amplitude, width, and period of 50 mV, 0.06, and 0.5 s, respectively. Samples were prepared as dichloromethane solutions, degassed by sparging with dichloromethane N2 for 5 minutes before measurements. All measurements were performed using 0.1 M dichloromethane solution of tetran-butylammonium hexafluorophosphate ([nBu4N]PF6]). An Ag/Ag+ electrode was used as the reference electrode, while a glassy carbon electrode and a platinum wire were used as the working electrode and counter electrode, respectively. The redox potentials are reported relative to a saturated calomel electrode (SCE) with a ferrocenium/ferrocene (Fc/Fc+) redox couple as the internal standard (0.46 V vs. SCE).[19]

The HOMO and LUMO energies were determined using the relation $E_{HOMO/LUMO} = -(E_{ox} / E_{red} + 4.8)$ eV, where E_{ox} and E_{red} are the onset of anodic and cathodic peak potentials, respectively calculated from DPV relative to Fc/Fc$^+$.[20]

Photophysical measurements. Optically dilute solutions of concentrations on the order of 10^{-5} or 10^{-6} M were prepared in spectroscopic or HPLC grade solvents for absorption and emission analysis. Absorption spectra were recorded at room temperature on a Shimazu UV-2600 double beam spectrophotometer with a 1 cm quartz cuvette. Molar absorptivity determination was verified by linear regression analysis of values obtained from at least four independent solutions at varying concentrations with absorbance ranging from 1.0×10^{-7} to 1×10^{-4} M. Steady-state and time-resolved emission spectra were recorded at 298 K using an Edinburgh Instruments FS5 and FLS980 spectrofluorometers. Samples were excited at 350 nm for steady-state measurements and at 378 nm for time-resolved measurements. For ΔE_{ST} measurements an open Dewar was used for solution samples. All samples were photoexcited using the third harmonic emission (343 nm) from a femtosecond Nd:YAG laser, which originally emits at 1030 nm (Orpheus-N, model: PN13F1). Emission from the samples was focused onto a spectrograph (Chromex imaging, 250is spectrograph) and detected on a sensitive gated iCCD camera (Stanford Computer Optics, 4Picos) having subnanosecond resolution. Phosphorescence spectra were measured 1 ms after the excitation of the Nd:YAG laser with iCCD exposure time of 8.5 ms. Prompt fluorescence spectra were measured 1 ns after the excitation of the femtosecond laser with iCCD exposure time of 100 ns. An integrating sphere (SC-30 module on FS5 fluorimeter) was employed for the photoluminescence quantum yield measurements of solid samples. The Φ_{PL} of the films were then measured for some cases in air and in all cases in N_2 environment by purging the integrating sphere with N_2 gas flow. The singlet-triplet energy splitting (ΔE_{ST}) in toluene was estimated from the onset of prompt fluorescence spectra and phosphorescence emission at 77 K. The samples were excited by a femtosecond laser emitting at 343 nm (Orpheus-N, model: SP-06-200-PP). Emission from the samples was focused onto a spectrograph (Chromex imaging, 250is spectrograph) and detected on a sensitive gated iCCD camera (Stanford Computer Optics, 4Picos) having subnanosecond resolution. Phosphorescence spectra of toluene glass were measured from 1 ms after photoexcitation, with an iCCD exposure time was 8.5 ms. Prompt fluorescence spectra were measured from 1 ns after photoexcitation with an iCCD exposure time was 100 ns.

2. Synthetic procedures and characterization data

Dimethyl 2,5-bis((4-(tert-butyl)phenyl)(2-(methoxycarbonyl)phenyl)amino)terephthalate (1):
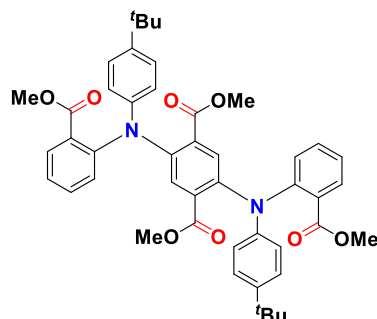
A 2-neck flask held under nitrogen was charged with 2,5-bis((4-(tert-butyl)phenyl)amino)terephthalate (4.00 g, 8.19 mmol, 1 equiv.), methyl 2-iodobenzoate (34.3 g, 19.2 mL, 131 mmol, 16 equiv.), copper (103 mg, 1.64 mmol, 0.2 equiv.) and anhydrous potassium carbonate (14.4 g, 12.7 mmol, 13 equiv.). The resulting reaction mixture was heated at 185 °C for 24 hours. After cooling to room temperature, the mixture was mixed with dichloromethane (50 mL) and washed with water (3 × 50 mL). The organic layer was then dried over anhydrous sodium sulfate and concentrated under reduced pressure. The resulting dark brown oil was purified by column chromatography on silica gel (CH₂Cl₂ only). The corresponding fractions were collected and evaporated under reduced pressure to afford the desired product as a brown reddish solid (8.80 g, 55%). **R$_f$**: 0.26 (CH$_2$Cl$_2$). Mp: 241–243 °C.
^{1}H NMR (400 MHz, Chloroform-*d*) δ 7.66 (dd, *J* = 7.7, 1.7 Hz, 2H), 7.47–7.43 (m, 2H), 7.42 (s, 2H), 7.25–7.21 (m, 6H), 7.17–7.13 (m, 2H), 6.80 (d, *J* = 8.7 Hz, 4H), 3.46 (s, 6H), 3.33 (s, 6H), 1.34–1.25 (m, 18H). **^{13}C NMR** (101 MHz, Chloroform-*d*) δ 167, 166, 146, 145, 145, 141, 132, 131, 131, 130, 128, 127, 125, 123, 121, 51, 51, 34, 31. **HR-MS [M+H]$^+$** Calculated: 757.3489 (C$_{46}$H$_{49}$N$_2$O$_8$); Found: 756.3411.

Sym-DiDiKTa and Asym-DiDiKTa:
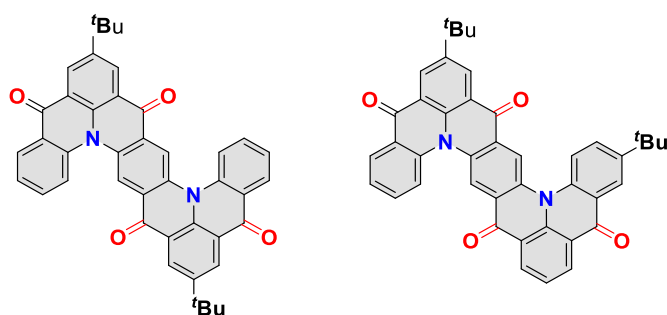
Compound **1** (4.3 g, 5.6 mmol, 1 equiv.) was combined with sodium hydroxide (2.2 g, 56 mmol, 10 equiv.) in 170 mL of an ethanol/water/tetrahydrofuran (1:1:3.5) mixture. The reaction was heated to reflux for 12 h. After cooling to room temperature, the pH was adjusted to 2-3 by addition of dilute hydrochloric acid. The tetra-acid precipitated as a brown greenish solid and was collected by vacuum filtration, washed thoroughly with water, dried under vacuum (4.9 g, 99% yield) and used without further purification and characterization. The tetra-acid (3.0 g, 4.3 mmol, 1 equiv.) was dispersed in 100 mL dichloromethane under a nitrogen atmosphere. To the reaction mixture were added sequentially thionyl chloride (20.4 g, 12.4 mL, 171 mmol, 40 equiv.) and 6 drops of *N,N*-dimethylformamide. After 3 h under reflux, the reaction mixture was cooled to room temperature. Under a positive flow of nitrogen, aluminium chloride (11.4 g, 85.6 mmol, 20 equiv.) was added slowly with stirring (exothermic reaction). After refluxing for 24 h, the reaction mixture was cooled to room temperature, and the reaction quenched by slow dropwise of water under vigorous stirring (exothermic reaction). The resulting mixture was combined with more dichloromethane (50 mL), the organic layer separated and washed with water (3 × 50 mL), and then dried over anhydrous sodium sulphate. The solvent was evaporated under reduced pressure and the brown solid crude product was purified by column chromatography on silica gel (5% EtOAc in CH_2Cl_2) to yield **Sym-DiDiKTa** (982 mg, 37%) and **Asym-DiDiKTa** (137 mg, 5%) both as orange solids.

Sym-DiDiKTa: R_f: 0.65 (5% EtOAc in CH_2Cl_2). **Mp**: > 390 °C. **^{1}H NMR** (400 MHz, Chloroform-*d*) δ 9.25 (s, 2H), 8.87 (d, *J* = 2.6 Hz, 2H), 8.78 (d, *J* = 2.5 Hz, 2H), 8.57 (dd, *J* = 7.9, 1.6 Hz, 2H), 8.31 (d, *J* = 8.5 Hz, 2H), 7.86–7.81 (m, 2H), 7.60–7.56 (m, 2H), 1.49 (s, 18H). **^{13}C NMR** (126 MHz, Chloroform-*d*) δ 178, 178, 147, 139, 137, 135, 133, 131, 130 128, 128, 126, 125, 123, 122, 119, 119, 35, 31. **Anal. Calcd. For $C_{42}H_{32}N_2O_4$.**: C, 80.24%; H, 5.13%; N, 4.46%. **Anal. Found**: C, 80.45%; H, 5.02%; N, 4.30. **HR-MS (ESI$^+$) [M+H]$^+$** Calculated:

629.2440 ($C_{42}H_{33}N_2O_4$); Found: 629.2431. 98.8% pure on HPLC analysis, retention time 2.4 minutes in 60% methanol 40% water.

Asym-DiDiKTa: R_f: 0.58 (5% EtOAc in CH_2Cl_2). **Mp**: 349 – 351 °C. **^{1}H NMR** (400 MHz, Chloroform-*d*) δ 9.28 (d, *J* = 9.6 Hz, 2H), 8.90 (d, *J* = 2.6 Hz, 1H), 8.86 (dd, *J* = 7.6, 1.6 Hz, 1H), 8.81 (d, *J* = 2.5 Hz, 1H), 8.76 (dd, *J* = 7.7, 1.8 Hz, 1H), 8.60–8.57 (m, 2H), 8.34 (d, *J* = 8.5 Hz, 1H), 8.27 (d, *J* = 8.9 Hz, 1H), 7.91 (dd, *J* = 8.9, 2.5 Hz, 1H), 7.88–7.84 (m, 1H), 7.69 (t, *J* = 7.7 Hz, 1H), 7.62–7.58 (m, 1H), 1.52–1.51 (m, 18H). **^{13}C NMR** (126 MHz, Chloroform-*d*) δ 178, 178, 178, 177, 149, 147, 139, 139, 137, 137, 135, 135, 134, 133, 133, 131, 131, 130, 128, 128, 126, 125, 125, 124, 123, 123, 123, 122, 122, 119, 119, 119, 119, 35, 35, 31, 31. **Anal. Calcd. For $C_{42}H_{32}N_2O_4$**: C, 80.24%; H, 5.13%; N, 4.46%. **Anal. Found**: C, 80.46%; H, 5.06%; N, 4.26; **LR-MS (MALDI[+]) [M+H][+]** Calculated: 629.2 ($C_{42}H_{33}N_2O_4$); Found: 629.2. 99.0% pure on HPLC analysis, retention time 2.3 minutes in 60% methanol 40% water.
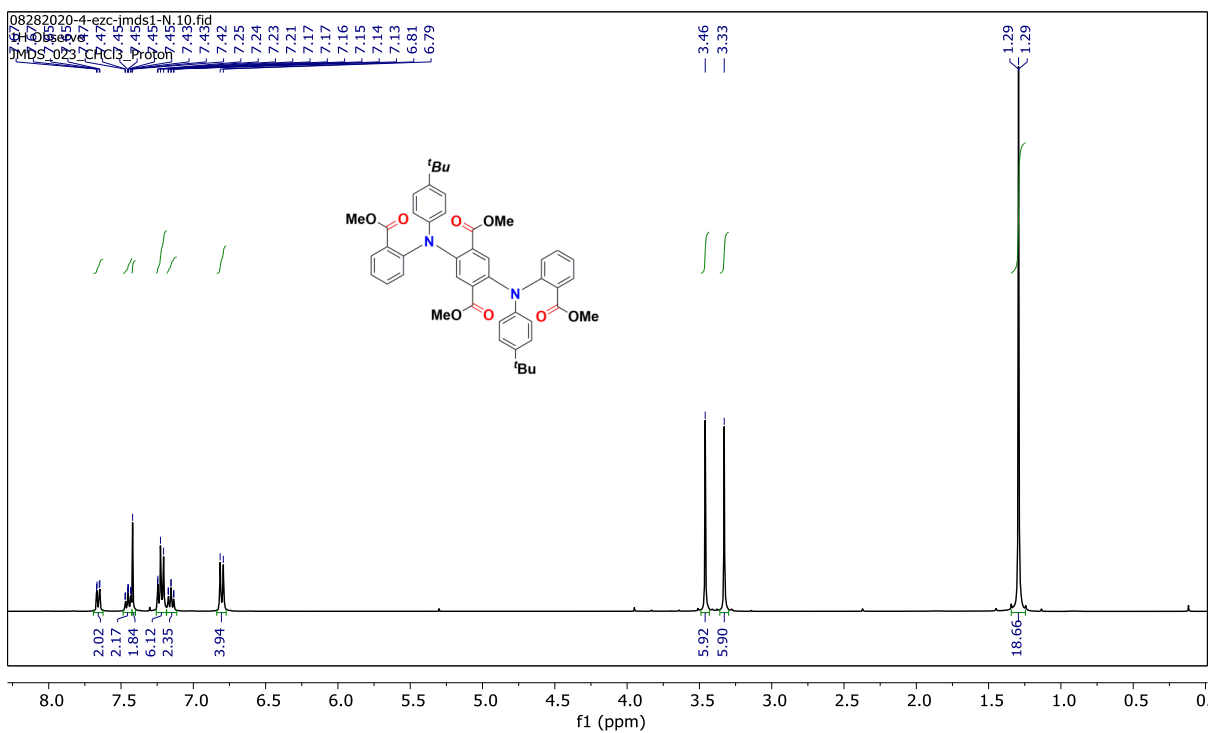
Figure S2. ^{1}H NMR (400 MHz, Chloroform-d) of compound **1**.
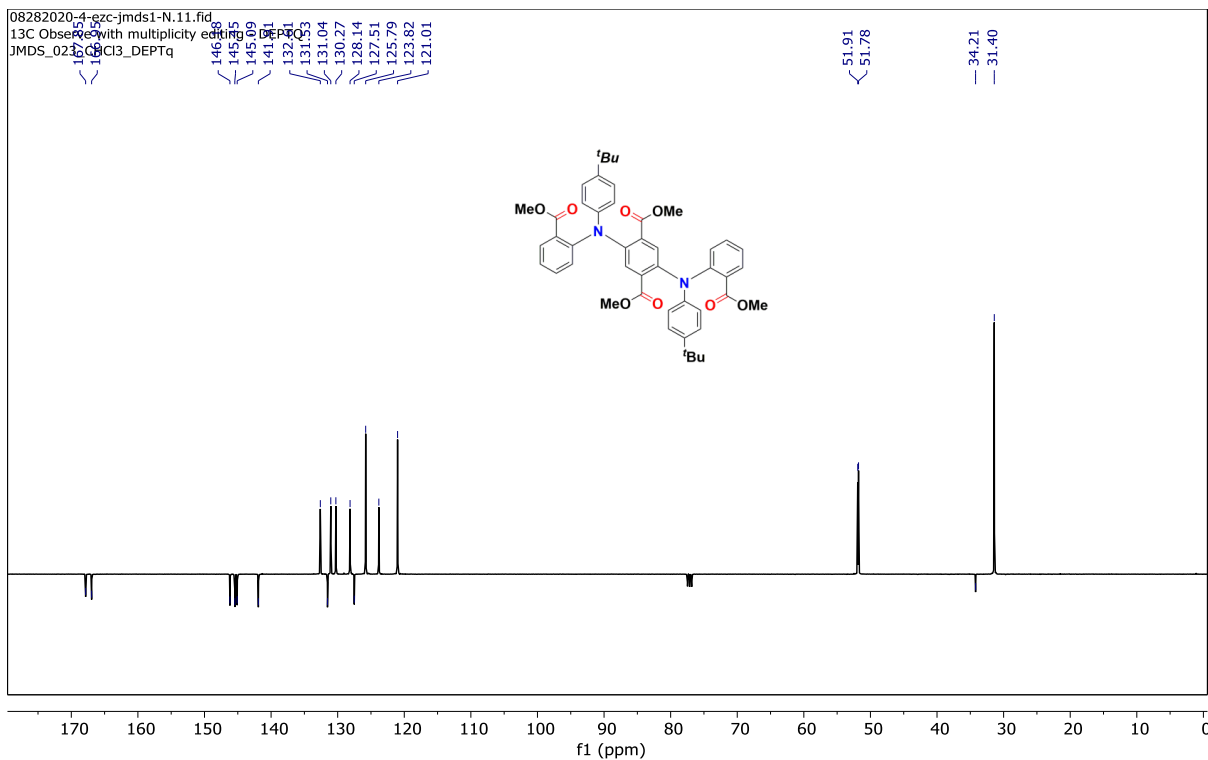
Figure S3. DEPTq-135 (101 MHz, Chloroform-d) of compound **1**.
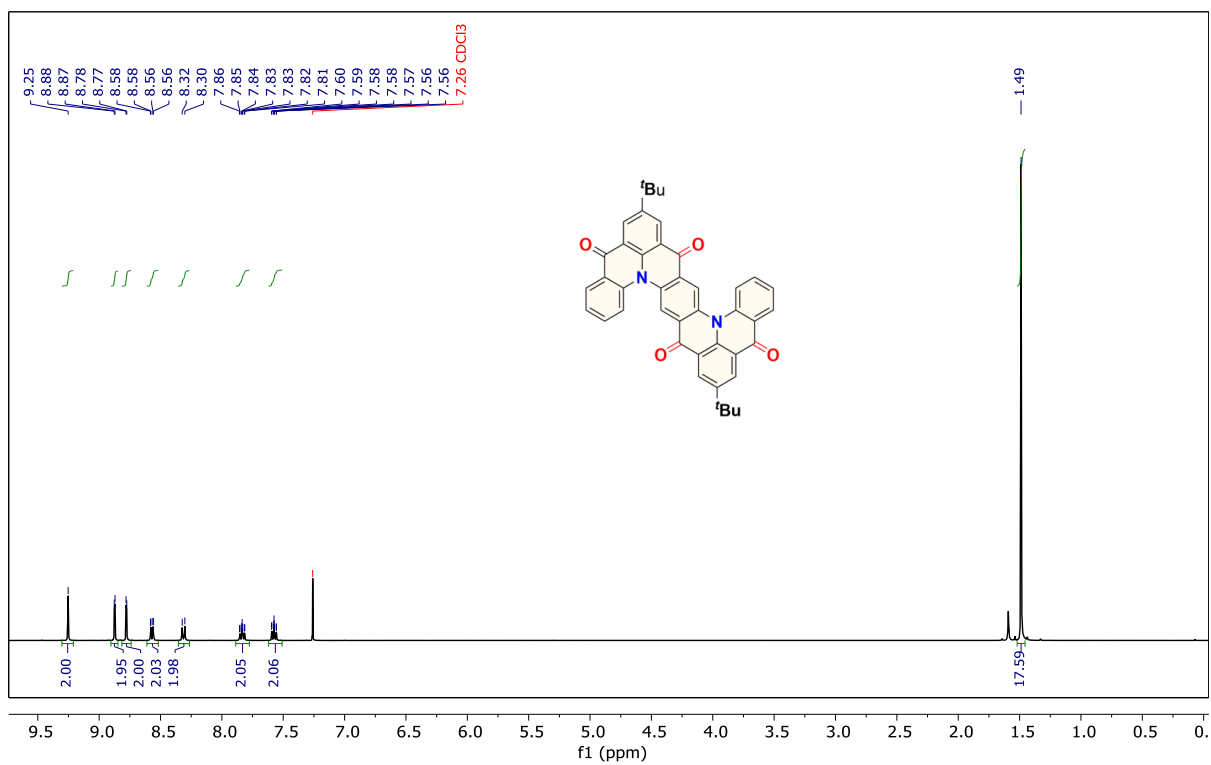
Figure S4. ^{1}H NMR (400 MHz, Chloroform-d) of **Sym-DiDiKTa**.
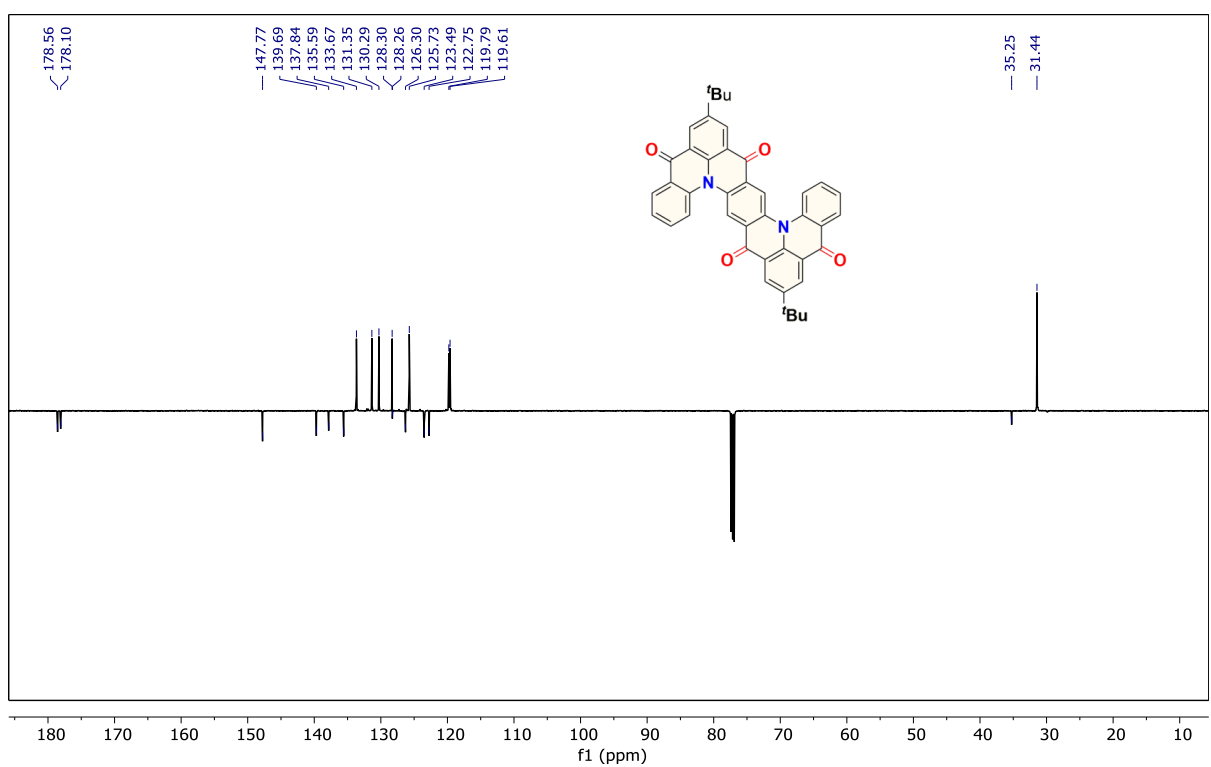
Figure S5. DEPTq-135 (126 MHz, Chloroform-d) of **Sym-DiDiKTa**.
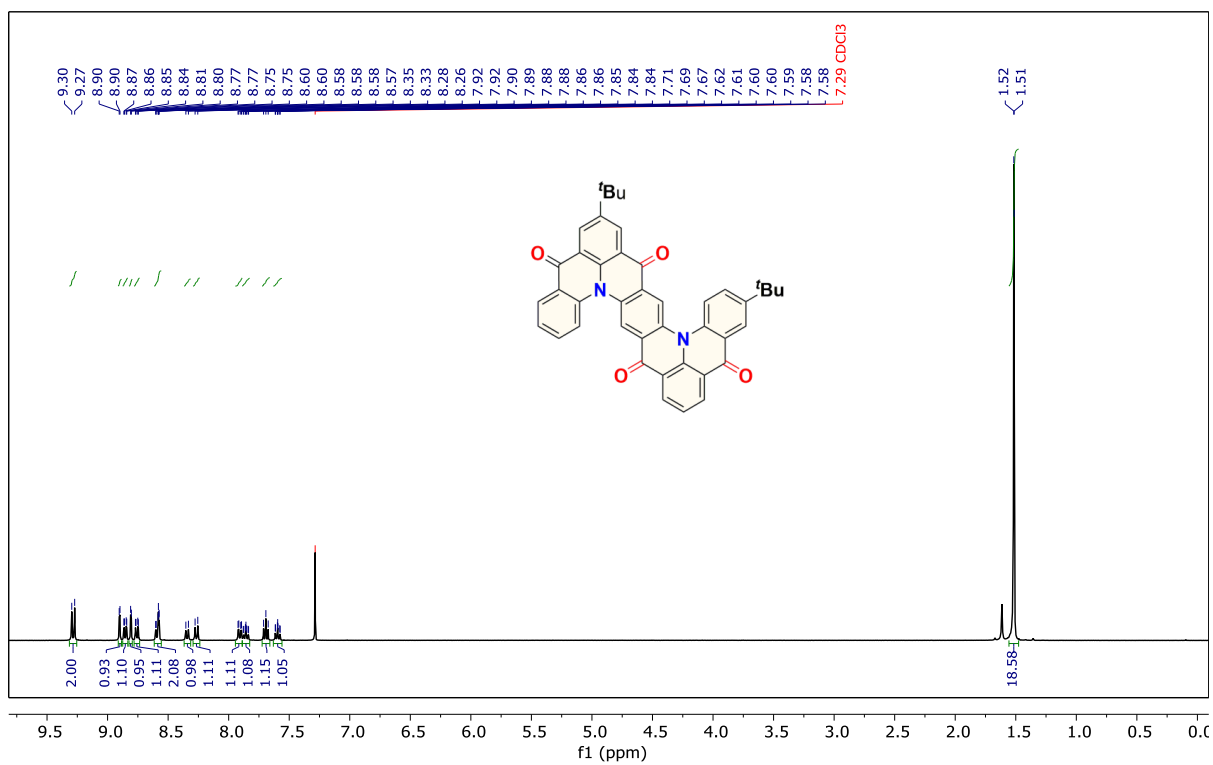
Figure S6. ^{1}H NMR (400 MHz, Chloroform-*d*) of **Asym-DiDiKTa**.
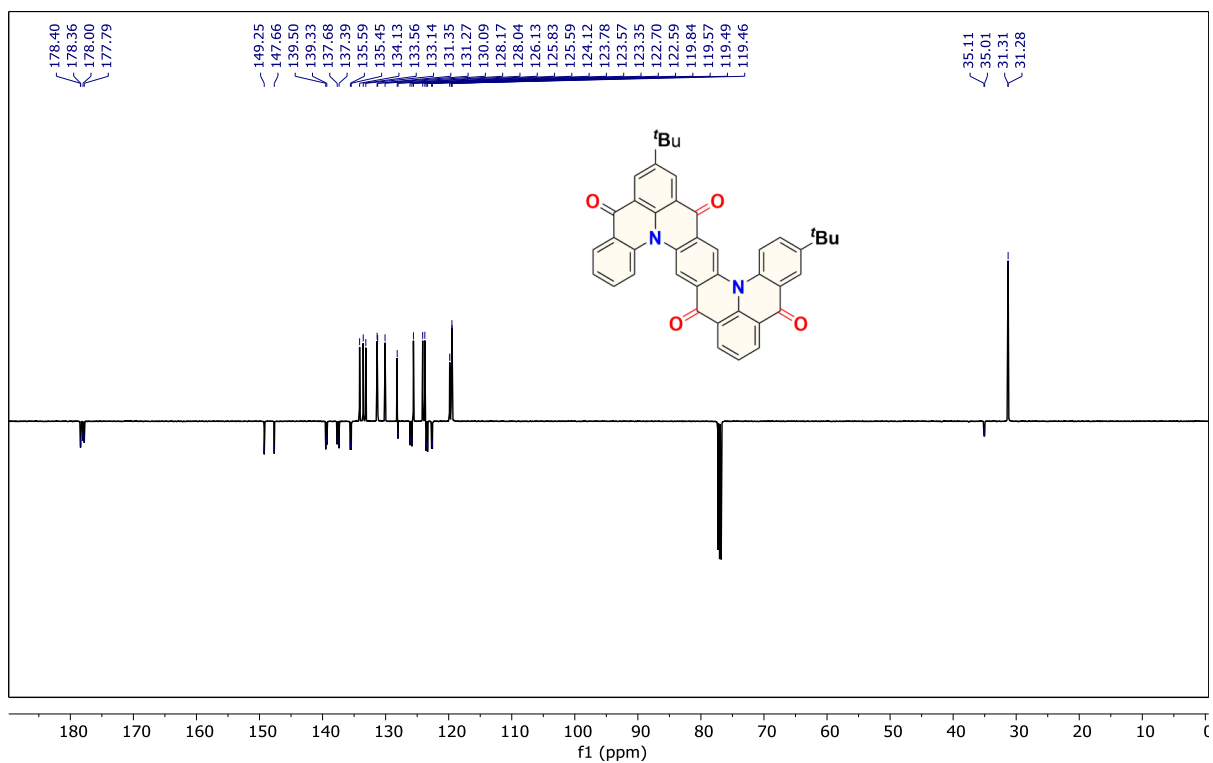
Figure S7. DEPTq-135 (126 MHz, Chloroform-*d*) of **Asym-DiDiKTa**.
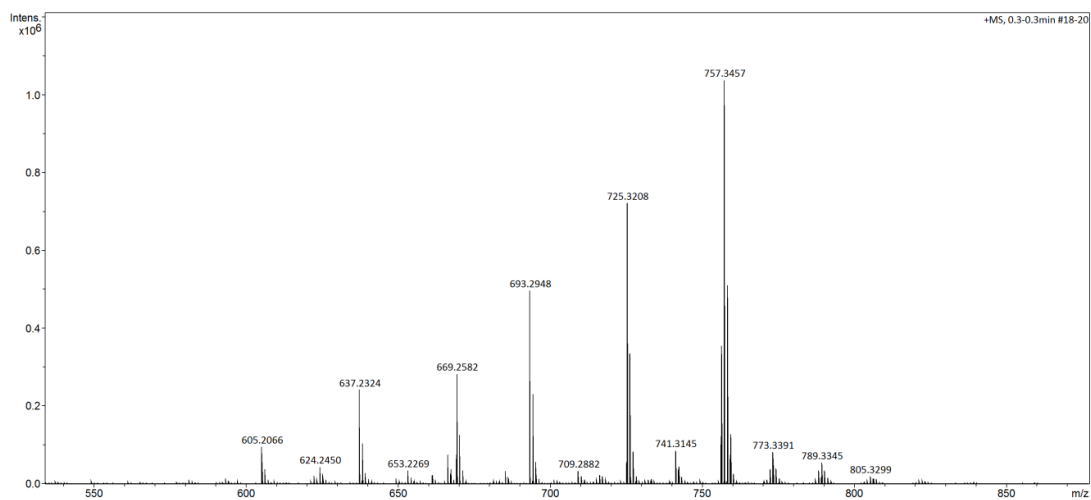
Figure S8. HRMS of compound **1**.
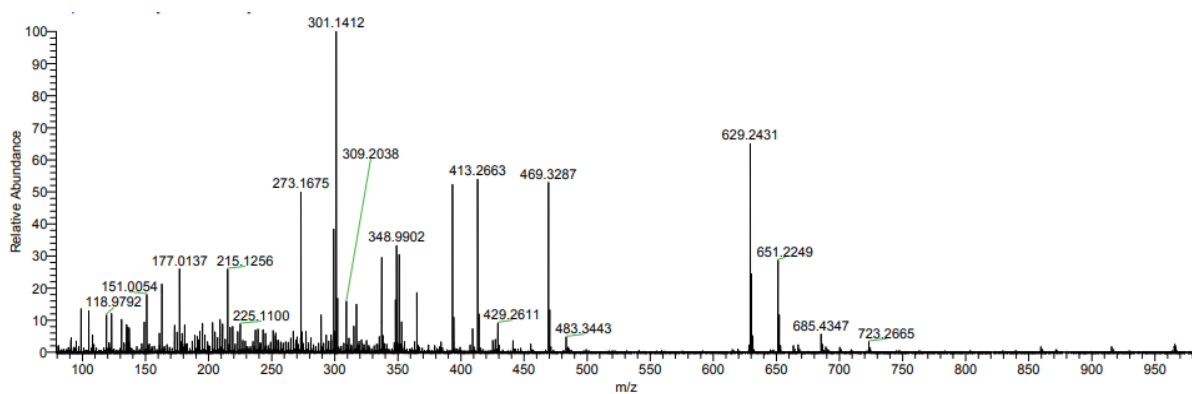
Figure S9. HRMS of **Sym-DiDiKTa**.
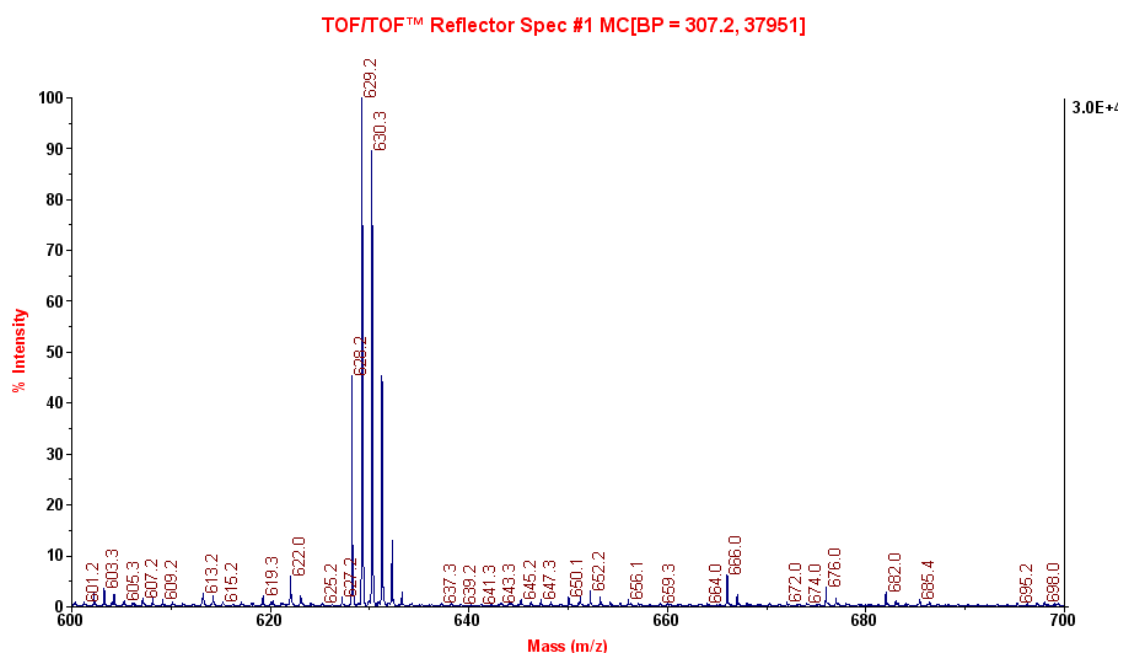
Figure S10. LRMS of **Asym-DiDiKTa**.

Figure S11. HPLC trace of **Sym-DiDiKTa**.

<Peak Table>
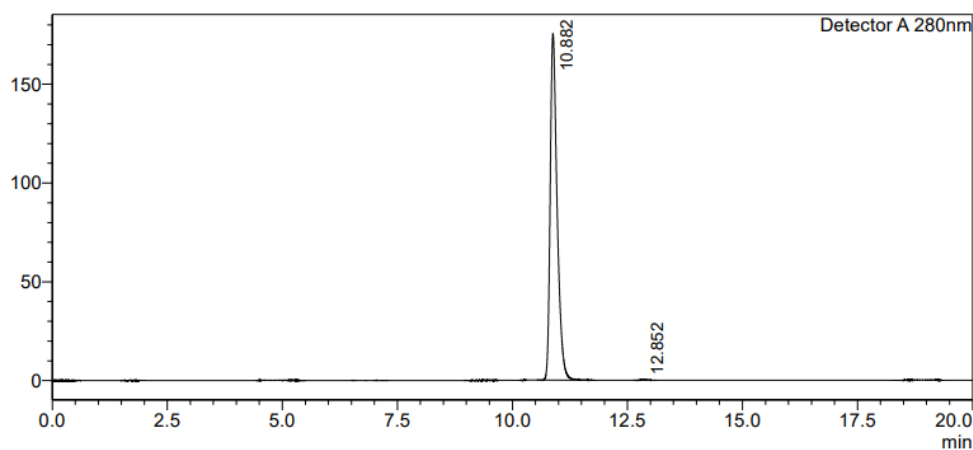
Detector A 280nm

Peak#	Ret. Time	Area	Height	Area%	Area/Height	Width at 5% Height
1	10.882	1836725	174927	99.697	10.500	0.372
2	12.852	5588	530	0.303	10.547	0.320
Total		1842313	175456	100.000		

<Peak Table>
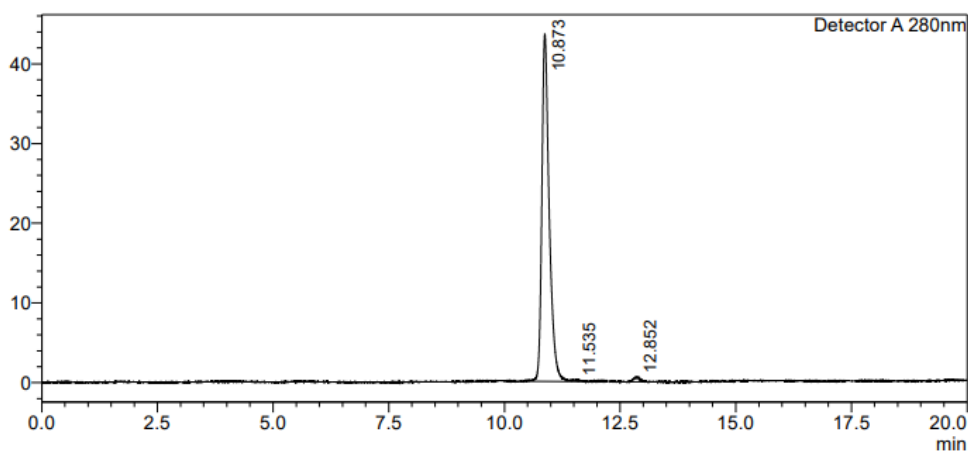
Detector A 280nm

Peak#	Ret. Time	Area	Height	Area%	Area/Height	Width at 5% Height
1	10.873	481741	43503	98.158	11.074	0.402
2	11.535	3045	207	0.620	14.723	--
3	12.852	5997	564	1.222	10.630	0.338
Total		490783	44274	100.000		

Figure S12. HPLC trace of **Asym-DiDiKTa**.

3. X-Ray Crystallography

X-ray diffraction data for **Sym-DiDiKTA** were collected using a Rigaku FR-X Ultrahigh Brilliance Microfocus RA generator/confocal optics with XtaLAB P200 diffractometer [Mo Kα radiation (λ = 0.71073 Å)]. Diffraction data for **Sym-DiDiKTA·MeOH** were collected using a Rigaku MM-007HF High Brilliance RA generator/confocal optics with XtaLAB P100 diffractometer [Cu Kα radiation (λ = 1.54187 Å)]. Data for **Asym-DiDiKTA** were collected using a Rigaku SCXmini CCD diffractometer with a SHINE monochromator [Mo Kα radiation (λ = 0.71073 Å)]. Intensity data were collected at 173 K, using either ω steps or both ω and φ steps accumulating area detector images spanning at least a hemisphere of reciprocal space. Data for all compounds were collected using CrystalClear[21] and processed (including correction for Lorentz, polarization and absorption) using CrysAlisPro.[22] Structures were solved by direct (SIR2004[23]) or dual-space (SHELXT[24]) methods and refined by full-matrix least-squares against F^2 (SHELXL-2018/3[25]). Non-hydrogen atoms were refined anisotropically, and hydrogen atoms were refined using a riding model. The structure of **Sym-DiDiKTA** showed rotational disorder in the orientation of a *t*Bu group. Methyl carbons were split over two sites with distance restraints applied to the minor component of the disorder. The same compound also showed non-merohedric twinning, with a twin law of [1 0 0.435 0 -1 0 0 0 -1] and a refined twin fraction of 0.33. All calculations were performed using the Olex2 interface.[26] Selected crystallographic data are presented in Table **S2**. Deposition numbers 2225501-2225503 contains the supplementary crystallographic data for this paper. These data are provided free of charge by the joint Cambridge Crystallographic Data Centre and Fachinformationszentrum Karlsruhe Access Structures service www.ccdc.cam.ac.uk/structures.

Table S2. Selected crystallographic data.

	Sym-DiDiKTA	Sym-DiDiKTA·MeOH	Asym-DiDiKTA
empirical formula	$C_{42}H_{32}N_2O_4$	$C_{43}H_{36}N_2O_5$	$C_{42}H_{32}N_2O_4$
fw	628.69	660.74	628.69
crystal description	Orange prism	Orange needle	Red prism
crystal size [mm^3]	0.11×0.07×0.03	0.21×0.02×0.01	0.18×0.09×0.08
space group	$P2_1/c$	$P\overline{1}$	$P\overline{1}$
a [Å]	10.6081(15)	7.7000(4)	7.4062(4)
b [Å]	15.326(2)	13.4077(10)	13.1648(7)
c [Å]	9.9716(13)	15.6654(7)	15.9136(8)
α [°]		83.189(5)	80.865(4)
β [°]	101.788(4)	89.665(4)	89.665(4)
γ [°]		81.607(5)	81.829(4)
vol [Å]^3	1587.0(4)	1588.56(16)	1516.14(14)
Z	2	2	2
ρ (calc) [g/cm^3]	1.316	1.381	1.377
μ [mm^{-1}]	0.085	0.725	0.089
F(000)	660	696	660
reflections collected	17782	16750	15677
independent reflections (R_{int})	2875 (0.0404)	5677 (0.0680)	6944 (0.0661)
parameters, restraints	252, 3	462, 1	439, 0
GOF on F^2	1.358	1.041	0.992
R_1 [$I > 2\sigma(I)$]	0.0680	0.0657	0.0612
wR_2 (all data)	0.2468	0.1855	0.1436
largest diff. peak/hole [e/Å^3]	0.299, -0.323	0.391, -0.276	0.229, -0.213
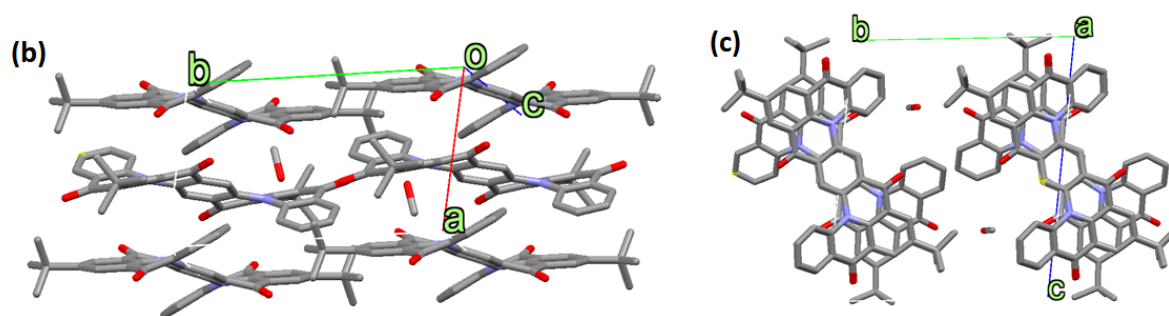
Figure 13. Crystal structure of **Sym-DiDiKTa** with MeOH incorporated in the unit cell: (a) diagonal view and (b) side view of the packing diagram.

4. Photophysical data
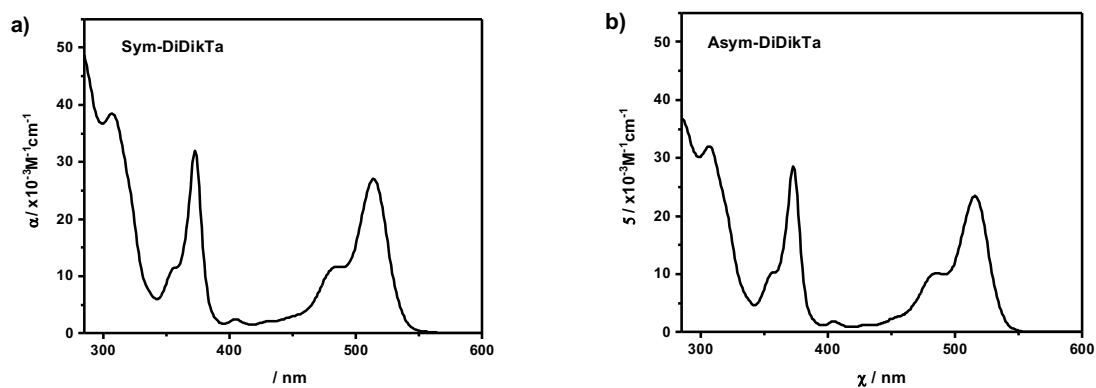
Figure S14. Absorption spectrum of **Sym-DiDiKTa** (a) and **Asym-DiDiKTa** (b), respectively, obtained in toluene (1.01×10^{-5} M) at 300 K.
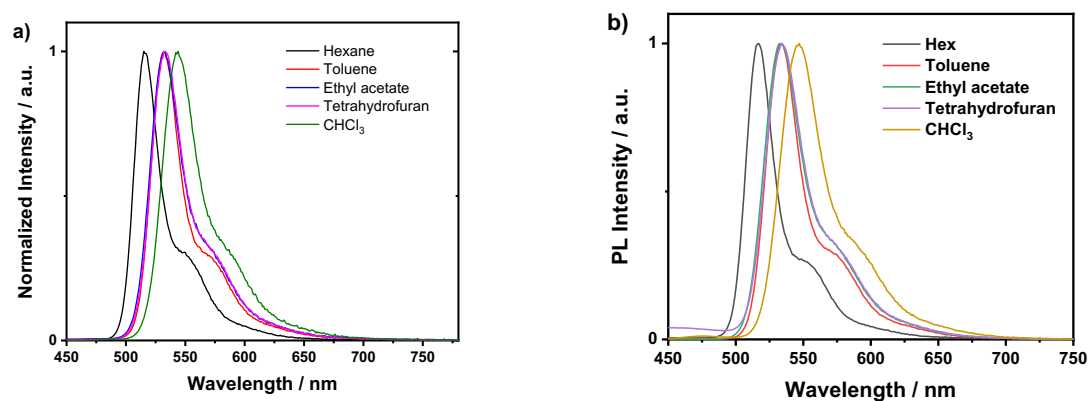
Figure S15. Solvatochromic PL study (λ_{exc} = 350 nm) of **Sym-DiDiKTa** (a) and **Asym-DiDiKTa** (b).
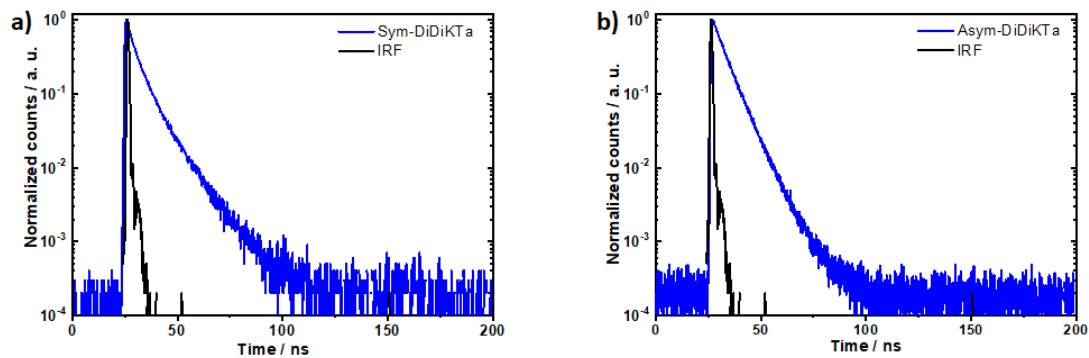
Figure S16. Room temperature time-resolved PL decays with a time window of 200 ns for 1 wt% **Sym-DiDiKTa** and **Asym-DiDiKTa**, respectively, in mCP matrix (λ_{exc} = 378 nm).
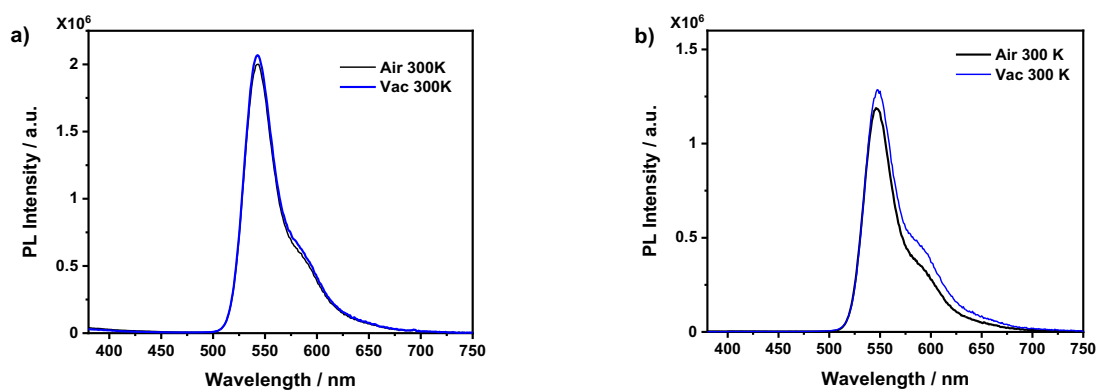
Figure S17. (a & b) SS PL spectra of **Sym-DiDiKTa** and **Asym-DiDiKTa**, respectively, in 1% in mCP in air and under vacuum at 300 K, λ_{exc} = 350 nm.

Table S3. Summary of solvatochromic PL properties of **Sym-DiDiKTa**.

Solvent	λ_{PL} [a]	FWHM [b]
	nm	nm / eV
Hexane (Hex)	515	25 / 0.11
Toluene (Tol)	531	29 / 0.12
Ethyl acetate (EA)	532	32 / 0.14
THF	532	33 / 0.14
CHCl$_3$	544	37 / 0.15

[a] Peak value of PL spectra obtained under aerated conditions at 300 K, concentration 1×10^{-5} M, λ_{exc} = 350 nm. [b] Full width at half maximum of the corresponding PL spectra.

Table S4. Summary of solvatochromic PL properties of **Asym-DiDiKTa**.

Solvent	λ_{PL} [a]	FWHM [b]
	nm	nm / eV
Hexane (Hex)	516	24 / 0.10
Toluene (Tol)	533	29 / 0.12
Ethyl acetate (EA)	532	34 / 0.15
THF	534	35 / 0.14
CHCl$_3$	546	38 / 0.15

[a] Peak value of PL spectra obtained under aerated conditions at 300 K, concentration 1×10^{-5} M, λ_{exc} = 350 nm. [b] Full width at half maximum of the corresponding PL spectra.

Table S5. Φ_{PL} study of **Sym-DiDiKTa** and **Asym-DiDiKTa** in different media, $\lambda_{exc} = 350$ nm.

Medium	$\Phi_{PL}(N_2*/Ar**)$ / %	$\Phi_{PL}(air)$ / %
Sym-DiDiKTa (in toluene) [a]	69.3*	64.7
Asym-DiDiKTa (in toluene) [a]	52.5*	49.7
Sym-DiDiKTa (0.5% in mCP) [b]	60**	-
Asym-DiDiKTa (0.5% in mCP) [b]	57**	-
Sym-DiDiKTa (1% in mCP) [b]	64**	-
Asym-DiDiKTa (1% in mCP) [b]	57**	-
1% **Sym-DiDiKTa** 20% HDT1 (in mCP) [b]	70**	-
1% **Sym-DiDiKTa** 20% HDT1 (in DPEPO) [b]	75**	-
1% **Sym-DiDiKTa** 20% 4CzIPN (in DPEPO) [b]	86**	-
1% **Sym-DiDiKTa** 20% 4CzIPN (in mCP) [b]	80**	-
1% **Sym-DiDiKTa** 20% 4CzIPN (in DPEPO) [b]	88**	-

[a] Film obtained *via* drop-casting. [b] Film obtained *via* vacuum deposition.

Table S6. S_1, T_1 and ΔE_{ST} values of **Sym-DiDiKTa** and **Asym-DiDiKTa**.[a]

	S_1 / eV	T_1 / eV	ΔE_{ST} / eV
Sym-DiDiKTa	2.33	2.11	0.22
Asym-DiDiKTa	2.33	2.12	0.21

[a] S_1, T_1 and ΔE_{ST} values of **Sym-DiDiKTa** and **Asym-DiDiKTa** calculated from the onsets of the prompt fluorescence (delay: 1 ns; gate time: 100 ns, λ_{exc} = 343 nm) and phosphorescence (delay: 1 ms; gate time: 8.5 ms, λ_{exc} = 343 nm) spectra in toluene glass at 77 K.

Table S7. Transient PL decay (MCS) data of 1 wt% **Sym-DiDiKTa** and **Asym-DiDiKTa** doped into mCP matrix at room temperature.[a]

Compound	τ_1 / µs	τ_2 / µs	τ_3 / µs	τ_4 / µs	A_1	A_2	A_3	A_4	R_1 %	R_2 %	R_3 %	R_4 %
Sym-DiDiKTa	1.8	141	986	5801	97096	384	85	23	39.6	12.1	18.6	29.7
Asym-DiDiKTa	1.6	86	416	2491	106093	140	78	42	53.5	3.8	10.1	32.6

[a] The transient PL decay data were fitted by quadruple-exponential function, where A_i is the pre-exponential for lifetime τ_i. R_i is individual component ratio for prompt and delayed fluorescence. $R_i = \tau_i A_i / \Sigma \tau_i A_i$. The data were obtained from MCS measurements, and an accurate lifetime of the prompt emission cannot be determined from such a long time window. A separate TCSPC measurement was performed for the evaluation of the prompt emission lifetime as shown in Figure **S16**.

Table S8. Summary of rate constants of **Sym-DiDiKTa** and **Asym-DiDiKTa** doped into mCP matrix at 300 K

Temperature	τ_p [a]	τ_d [b]	k_r^{S} [c]	k_{ISC} [d]	k_{RISC} [e]	k_{nr}^{S} [f]
/K	/ ns	/ ms	/ $\times 10^7$ s^{-1}	/ $\times 10^7$ s^{-1}	/ $\times 10^3$ s^{-1}	/ $\times 10^7$ s^{-1}
Sym-DiDiKTa	1.7	4.6	2.7	4.1	7.0	3.8
Asym-DiDiKTa	8.3	3.0	3.1	2.7	5.6	4.4

[a] Average lifetime of prompt emission; [b] Average lifetime of delayed emission; [c] radiative decay rate constant of singlet excitons; [d] intersystem crossing rate constant; [e] reverse intersystem crossing rate constant; [f] nonradiative decay rate constant of singlet excitons.

Rate constant calculations

The constants (k_r and k_{nr}) for prompt and delayed emission can be estimated according to their contributions to total Φ_{PL} and their lifetimes (τ_p and τ_d) according to the quadruple exponential fitting of time-resolved decay curves at 300 K. To determine the rates, we used the following equations according to previous studies[27] of TADF photophysical processes:

$$k_r^{S} = \Phi_p \times k_p \qquad (1)$$

$$k_{ISC} = (\Phi_{PL} - \Phi_p) \times k_p \qquad (2)$$

$$k_{RISC} = \frac{k_d \times \Phi_d}{(\Phi_{PL} - \Phi_p) \times 1} \qquad (3)$$

$$k_{nr}^{S} = (1 - \Phi_{PL}) \times k_p \qquad (4)$$

where Φ_{PL} is the absolute Φ_{PL}; Φ_p and Φ_d are the prompt and delayed fluorescence efficiencies, respectively; k_p and k_d are the prompt and delayed fluorescence decay rate, respectively; τ_p and τ_d are the average lifetimes of prompt and delayed fluorescence; nr, ISC and RISC are non-radiative, intersystem crossing, and reverse intersystem crossing processes.

Table S9. Electrochemical data of **Sym-DiDiKTa** and **Asym-DiDiKTa** compared to the parent **DiKTa**.[2]

Compound	E_{ox} [a]	E_{red} [a]	HOMO [b]	LUMO [b]	ΔE [c]
	/ V	/ V	/ eV	/ eV	/ eV
Sym-DiDiKTa	1.53	-0.96	-5.87	-3.38	2.49
Asym-DiDiKTa	1.53	-0.94	-5.87	-3.40	2.47
DiKTa	1.66[2]	-1.33[2]	-5.93[2]	-3.11[2]	2.82[2]

[a] Potential values obtained for **Sym-DiDiKTa** and **Asym-DiDiKTa** from the DPV peak values, measured in degassed dichloromethane with 0.1 M [^{n}Bu$_4$N]PF$_6$ as the supporting electrolyte and referenced with respect to SCE (Fc/Fc$^+$ = 0.46 eV).[19] [b] HOMO and LUMO energy levels determined using the relation $E_{HOMO/LUMO} = -(E_{ox} / E_{red} + 4.8)$ eV (using Fc/Fc$^+$ as the internal reference);[20] [c] $\Delta E = |HOMO - LUMO|$ eV. [2] Value obtained from the literature in MeCN.

5. Quantum chemical calculations

The calculations were performed with the Gaussian 16 revision A_03[28] suite for the density functional theory (DFT) and with the Turbomole/7.4[29] package for SCS-CC2 calculations. Ground-state optimized structures were calculated using the PBE0 functional[30] and the 6-31G(d,p) basis set.[31] Molecular orbitals were visualized using GaussView 5.0 software.[32] Spin-component scaling coupled-cluster singles-and-doubles model (SCS-CC2) was also used in conjunction with cc-pVDZ basis set.[33] We first optimized the ground state using SCS-CC2 method, then vertical excited states were performed on the ground state optimized structure using the SCS-CC2 method. Difference density plots were used to visualize change in electronic density between the ground and excited state and were visualized using the VESTA package.

Table S11. Computational data calculated in the gas phase for **Sym-DiDiKTa**, **Asym-DiDiKTa** and **DiKTa**.

Compound	HOMO / eV[a]	LUMO / eV[a]	ΔE / eV[b]	S_1 / eV (f)	T_1 / eV	T_2 / eV	ΔE_{ST} / eV
Sym-DiDiKTa	-5.94	-2.69	3.25	2.93 (0.26)	2.69	3.15	0.24
Asym-DiDiKTa	-5.94	-2.69	3.25	2.93 (0.27)	2.69	3.16	0.24
DiKTa	-6.20	-2.23	3.97	3.45 (0.20)	3.18	3.60	0.27

[a]Calculated from PBE0/6-31G(d,p), [b] ΔE = LUMO – HOMO.
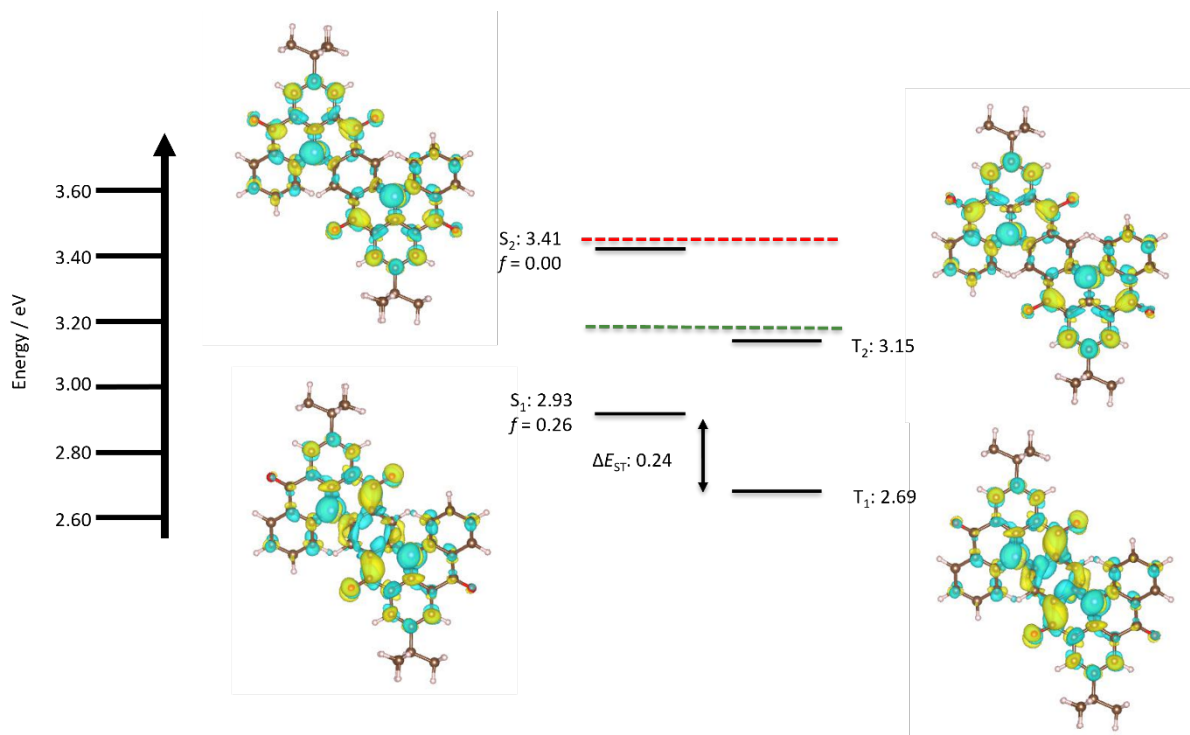
Figure S18. Difference density picture and excited state energies of **Sym-DiDiKTa** calculated at SCS-CC2/cc-pVDZ level, where red and green dotted lines represent calculated S_1 and T_1 energies repectively of **DiKTa**, (isovalue = 0.001).

Figure S19. Difference density picture and excited state energies of **Asym-DiDiKTa** calculated at SCS-CC2/cc-pVDZ level, where red and green dotted lines represent calculated S_1 and T_1 energies respectively of **DiKTa**, (isovalue = 0.001).

LUMO: -2.69 EV   LUMO: - 2.69 EV

HOMO: -5.94 EV   HOMO: -5.94 EV

Sym-DiDiKTa   **Asym-DiDiKTa**
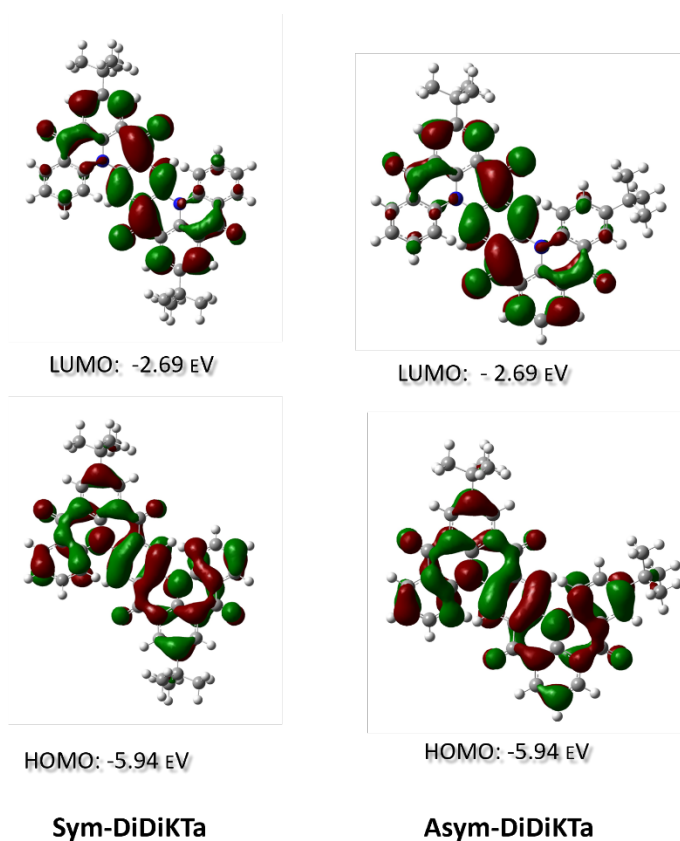
Figure S20. HOMO/LUMO electron density pictures and energies of **Sym-DiDiKTa** and **Asym-DiDiKTa** in the gas phase calculated with PBE0/6-31G(d,p), isovalue = 0.02.

Table S12. Calculated singlet excited states using SCS-CC2/cc-pVDZ, where f is oscillator strength.

Compound	S_1 (f) / eV	S_2 (f) / eV	S_3 (f) / eV	S_4 (f) / eV	S_5 (f) / eV	S_6 (f) / eV
Sym-DiDiKTa	2.93 (0.26)	3.41 (0.00)	3.76 (0.00)	3.84 (0.25)	3.88 (0.06)	4.17 (0.20)
Asym-DiDiKTa	2.93 (0.27)	3.41 (0.00)	3.73 (0.00)	3.76 (0.00)	3.83 (0.25)	3.87 (0.00)
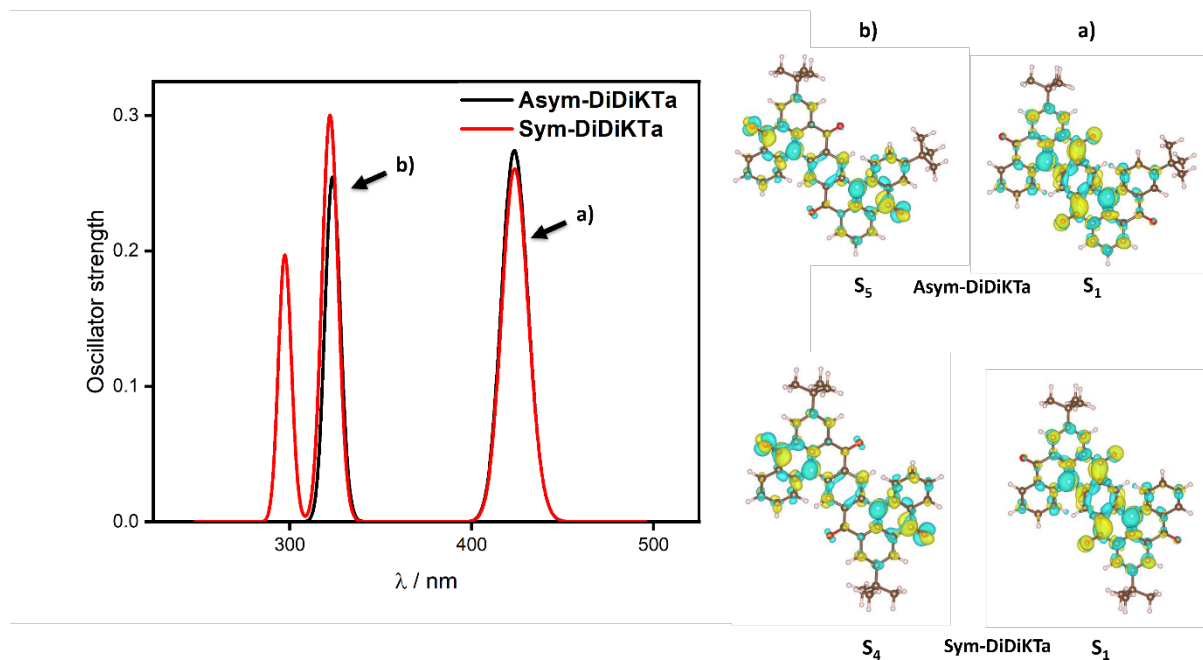
Figure S21. Simulated absorption spectra of **Asym-DiDiKTa** and **SymDiDiKTa** calculated from the first six singlet excited states from SCS-CC2 (FWHM = 0.05 eV), and difference density plots of the key transitions, (isovalue = 0.001).

6. OLED characterization

The OLEDs were fabricated through vacuum deposition of the materials at ca. 10^{-5} Pa onto indium tin oxide-coated glass substrates having a sheet resistance of ca. 15 Ω per □. The indium tin oxide surface was cleaned ultrasonically and sequentially with acetone, *iso*propanol and deionized water, then dried in an oven, and finally exposed to ultraviolet light and ozone for about 10 min. Organic layers were deposited at a rate of 1–2 Å/s. Subsequently, Liq was deposited at 0.1–0.2 Å/s. The devices were exposed once to nitrogen gas after the formation of the organic layers to allow the fixing of a metal mask to define the cathode area. For all OLEDs, the emitting areas were determined by the overlap of two electrodes as 0.04 cm^2. The J-V-luminance characteristics were evaluated using a Keithley 2400 source meter and an absolute external quantum efficiency (EQE) measurement system (C9920-12, Hamamatsu Photonics, Japan).

7. LEC fabrication and characterization
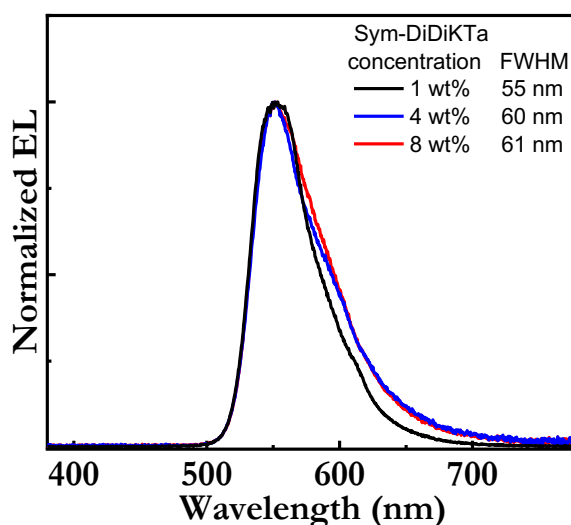
Figure S22. The steady-state EL spectrum of the blend-host:guest LEC for three different guest concentrations, as identified in the inset. The inset also presents the corresponding values for the FWHM.

The active-material ink was prepared by dissolving the constituents in chlorobenzene in a total concentration of 40 g/L by stirring on a magnetic hot at 90 °C plate for 3 h. The LEC devices were fabricated by sequentially spin-coating indium tin oxide-coated glass substrates with first a poly(3,4-ethylenedioxythiophene) polystyrene sulfonate ink (Clevios P VP AI4083, Heraeus) at 4000 rpm for 60 s and then the active-material ink at 2000 rpm for 60 s. A set of four Al cathodes was deposited on top of the active material by thermal evaporation under vacuum ($p < 5 \times 10^{-4}$ Pa). The light-emission area was 0.85×0.15 cm^2, as defined by the overlap between the anode and the cathode. All of the above procedures, except for the deposition of the PEDOT:PSS layer, were carried out in two interconnected N_2-filled glove boxes ($[O_2] < 1$ ppm, $[H_2O] < 0.5$ ppm). The LEC devices were characterized with a computer-controlled source-measure unit (Agilent U2722A) and a calibrated photodiode, equipped with an eye-response filter (S9219-01, Hamamatsu Photonics), connected to an embedded evaluation board (myRIO-1900, National Instruments) *via* a current-to-voltage amplifier. The EL spectra were recorded with a calibrated fiber-optic spectrometer (USB2000+, Ocean Optics).

References

1.   Yuan, Y.; Tang, X.; Du, X. Y.; Hu, Y.; Yu, Y. J.; Jiang, Z. Q.; Liao, L. S.; Lee, S. T., The Design of Fused Amine/Carbonyl System for Efficient Thermally Activated Delayed Fluorescence: Novel Multiple Resonance Core and Electron Acceptor. *Advanced Optical Materials* **2019,** *7* (7), 6-11.

2.   Hall, D.; Suresh, S. M.; dos Santos, P. L.; Duda, E.; Bagnich, S.; Pershin, A.; Rajamalli, P.; Cordes, D. B.; Slawin, A. M. Z.; Beljonne, D.; Köhler, A.; Samuel, I. D. W.; Olivier, Y.; Zysman-Colman, E., Improving Processability and Efficiency of Resonant TADF Emitters: A Design Strategy. *Advanced Optical Materials* **2020,** *8* (2), 1901627-1901627.

3.   Li, X.; Shi, Y. Z.; Wang, K.; Zhang, M.; Zheng, C. J.; Sun, D. M.; Dai, G. L.; Fan, X. C.; Wang, D. Q.; Liu, W.; Li, Y. Q.; Yu, J.; Ou, X. M.; Adachi, C.; Zhang, X. H., Thermally Activated Delayed Fluorescence Carbonyl Derivatives for Organic Light-Emitting Diodes with Extremely Narrow Full Width at Half-Maximum. *ACS Applied Materials and Interfaces* **2019,** *11* (14), 13472-13480.

4.   Sun, D.; Suresh, M.; Hall, D.; Zhang, M.; Si, C.; Cordes, D. B.; Slawin, A. M. Z.; Olivier, Y.; Zhang, X.; Zysman-colman, E., The design of an extended multiple resonance TADF emitter based on a polycyclic amine/carbonyl system. *Materials Chemistry Frontiers* **2020,** *4*, 2018-2022.

5.   Qiu, X.; Tian, G.; Lin, C.; Pan, Y.; Ye, X.; Wang, B.; Ma, D.; Hu, D.; Luo, Y.; Ma, Y., Narrowband Emission from Organic Fluorescent Emitters with Dominant Low-Frequency Vibronic Coupling. *Advanced Optical Materials* **2020,** *9* (4), 2001845-2001845.

6.   Huang, F.; Wang, K.; Shi, Y. Z.; Fan, X. C.; Zhang, X.; Yu, J.; Lee, C. S.; Zhang, X. H., Approaching Efficient and Narrow RGB Electroluminescence from D-A-Type TADF Emitters Containing an Identical Multiple Resonance Backbone as the Acceptor. *ACS Applied Materials and Interfaces* **2021,** *13* (30), 36089-36097.

7.   Zou, S.-n.; Peng, C.-c.; Yang, S.-y.; Qu, Y.-k.; Yu, Y.-j.; Chen, X.; Jiang, Z.-q.; Liao, L.-s., Fully Bridged Triphenylamine Derivatives as Color-Tunable Thermally Activated Delayed Fluorescence Emitters. *Organic Letters* **2021,** *23* (3), 958–962.

8.   Hamzehpoor, E.; Perepichka, D. F., Crystal Engineering of Room Temperature Phosphorescence in Organic Solids. *Angewandte Chemie - International Edition* **2020,** *59* (25), 9977-9981.

9.   Tsuchiya, Y.; Ishikawa, Y.; Lee, S. H.; Chen, X. K.; Brédas, J. L.; Nakanotani, H.; Adachi, C., Thermally Activated Delayed Fluorescence Properties of Trioxoazatriangulene Derivatives Modified with Electron Donating Groups. *Advanced Optical Materials* **2021,** *9* (14), 2002174-2002174.

10.   Wang, K.; Fan, X.-C.; Tsuchiya, Y.; Shi, Y.-Z.; Tanaka, M.; Lin, Z.; Lee, Y.-t.; Zhang, X.; Liu, W.; Dai, G.-l.; Chen, J.-X.; Wu, B.; Zhong, J.; Jian, Y.; Zheng, C.-J.; Yu, J.; Lee, C.-S.; Adachi, C.; Zhang, X.-H., Efficient and high colour purity RGB OLEDs employing densely packed dimers. *ChemRxiv. Cambridge: Cambridge Open Engage* **2021**.

11.   Min, H.; Park, I. S.; Yasuda, T., cis‐Quinacridone‐Based Delayed Fluorescence Emitters: Seemingly Old but Renewed Functional Luminogens. *Angewandte Chemie International Edition* **2021,** *60* (14), 7643-7648.

12.   dos Santos, J. M.; Sun, D.; Moreno-Naranjo, J. M.; Hall, D.; Zinna, F.; Ryan, S. T. J.; Shi, W.; Matulaitis, T.; Cordes, D. B.; Slawin, A. M. Z.; Beljonne, D.; Warriner, S. L.; Olivier, Y.; Fuchter, M. J.; Zysman-Colman, E., An S-shaped double helicene showing both multi-resonance thermally activated delayed fluorescence and circularly polarized luminescence. *Journal of Materials Chemistry C* **2022,** *10*, 4861-4870.

13.   Yang, S.-Y.; Zou, S.-N.; Kong, F.-C.; Liao, X.-J.; Qu, Y.-K.; Feng, Z.-Q.; Zheng, Y.-X.; Jiang, Z.-Q.; Liao, L.-S., A narrowband blue circularly polarized thermally activated delayed fluorescence emitter with a hetero-helicene structure. *Chemical Communications* **2021,** *57* (84), 11041-11044.

14.   Yang, S.-Y.; Tian, Q.-S.; Liao, X.-J.; Wu, Z.-G.; Shen, W.-S.; Yu, Y.-J.; Feng, Z.-Q.; Zheng, Y.-X.; Jiang, Z.-Q.; Liao, L.-S., Efficient circularly polarized thermally activated delayed fluorescence hetero-

[4]helicene with carbonyl-/sulfone-bridged triarylamine structures. *Journal of Materials Chemistry C* **2022,** *10* (11), 4393-4401.

15.   Wu, S.; Li, W.; Yoshida, K.; Hall, D.; Madayanad Suresh, S.; Sayner, T.; Gong, J.; Beljonne, D.; Olivier, Y.; Samuel, I. D. W.; Zysman-Colman, E., Excited-State Modulation in Donor-Substituted Multiresonant Thermally Activated Delayed Fluorescence Emitters. *ACS Applied Materials & Interfaces* **2022,** *14* (19), 22341-22352.

16.   Wu, S.; Gupta, A. K.; Yoshida, K.; Gong, J.; Hall, D.; Cordes, D. B.; Slawin, A. M. Z.; Samuel, I. D. W.; Zysman-Colman, E., Highly Efficient Green & Red Narrowband Emissive Organic Light-Emitting Diodes Employing Multi-Resonant Thermally Activated Delayed Fluorescence Emitters. *Angewandte Chemie - International Edition* **2022,** *61* (52), e202213697.

17.   Luo, X. F.; Li, F. L.; Zou, J. W.; Zou, Q.; Su, J.; Mao, M. X.; Zheng, Y. X., A Series of Fused Carbazole/Carbonyl Based Blue to Yellow‑Green Thermally Activated Delayed Fluorescence Materials for Efficient Organic Light‑Emitting Diodes. *Advanced Optical Materials* **2021,** *9* (21).

18.   Liu, J.-F.; Zou, S.-N.; Chen, X.; Yang, S.-Y.; Yu, Y.-J.; Fung, M.-K.; Jiang, Z.-Q.; Liao, L.-S., Isomeric thermally activated delayed fluorescence emitters based on a quinolino[3,2,1-de]acridine-5,9-dione multiple resonance core and carbazole substituent. *Materials Chemistry Frontiers* **2022,** *6* (7), 966-972.

19.   Connelly, N. G.; Geiger, W. E., Chemical redox agents for organometallic chemistry. *Chemical Reviews* **1996,** *96* (2), 877-910.

20.   Cardona, C. M.; Li, W.; Kaifer, A. E.; Stockdale, D.; Bazan, G. C., Electrochemical considerations for determining absolute frontier orbital energy levels of conjugated polymers for solar cell applications. *Advanced Materials* **2011,** *23* (20), 2367-2371.

21.   *CrystalClear-SM Expert v2.1.*, Rigaku Americas, The Woodlands, Texas, USA, and Rigaku Corporation: Tokyo, Japan, 2015.

22.   *CrysAlisPro v1.171.40.14a and v1.171.41.93a.* , Rigaku Oxford Diffraction, Rigaku Corporation: Oxford, U.K., 2018-2020.

23.   Burla, M. C.; Caliandro, R.; Camalli, M.; Carrozzini, B.; Cascarano, G. L.; De Caro, L.; Giacovazzo, C.; Polidori, G.; Spagna, R., An Improved Tool for Crystal Structure Determination and Refinement. *Journal of Applied Crystallography* **2005,** *38*, 381-388.

24.   Sheldrick, G. M., SHELXT– Integrated space-group and crystal structure determination *Acta Crystallographica* **2015,** *71*, 3-8.

25.   Sheldrick, G. M., Crystal structure refinement with SHELXL. *Acta Crystallographica. Sect. C.* **2015,** *71*, 3-8.

26.   Dolomanov, O. V.; Bourhis, L. J.; Gildea, R. J.; Howard, J. A. K.; Puschmann, H., OLEX2: A Complete Structure Solution, Refinement and Analysis Program. *Journal of Applied Crystallography* **2009,** *42*, 339-341.

27.   Tsuchiya, Y.; Diesing, S.; Bencheikh, F.; Wada, Y.; dos Santos, P. L.; Kaji, H.; Zysman-Colman, E.; Samuel, I. D. W.; Adachi, C., Exact Solution of Kinetic Analysis for Thermally Activated Delayed Fluorescence Materials. *Journal of Physical Chemistry A* **2021,** *125* (36), 8074-8089.

28.   Frisch, M. J.; Trucks, G. W.; Schlegel, H. B.; Scuseria, G. E.; Robb, M. A.; Cheeseman, J. R.; Scalmani, G.; Barone, V.; Petersson, G. A.; Nakatsuji, H.; Li, X.; Caricato, M.; Marenich, A. V.; Bloino, J.; Janesko, B. G.; Gomperts, R.; Mennucci, B.; Hratchian, H. P.; Ortiz, J. V.; Izmaylov, A. F.; Sonnenberg, J. L.; Williams-Young, D.; Ding, F.; Lipparini, F.; Egidi, F.; Goings, J.; Peng, B.; Petrone, A.; Henderson, T.; Ranasinghe, D.; Zakrzewski, V. G.; Gao, J.; Rega, N.; Zheng, G.; Liang, W.; Hada, M.; Ehara, M.; Toyota, K.; Fukuda, R.; Hasegawa, J.; Ishida, M.; Nakajima, T.; Honda, Y.; Kitao, O.; Nakai, H.; Vreven, T.; Throssell, K.; Montgomery, J. A.; Jr; Peralta, J. E.; Ogliaro, F.; Bearpark, M. J.; Heyd, J. J.; Brothers, E. N.; Kudin, K. N.; Staroverov, V. N.; Keith, T. A.; Kobayashi, R.; Normand, J.; Raghavachari, K.; Rendell, A. P.; Burant, J. C.; Iyengar, S. S.; Tomasi, J.; Cossi, M.; Millam, J. M.; Klene, M.; Adamo, C.; Cammi, R.; Ochterski, J. W.; Martin, R. L.; Morokuma, K.; Farkas, O.; Foresman, J. B.; Fox, D. J., Gaussian 16, Revision C.01. Gaussian, Inc.: Wallingford CT, 2016.

29.   Balasubramani, S. G.; Chen, G. P.; Coriani, S.; Diedenhofen, M.; Frank, M. S.; Franzke, Y. J.; Furche, F.; Grotjahn, R.; Harding, M. E.; Hättig, C.; Hellweg, A.; Helmich-Paris, B.; Holzer, C.; Huniar, U.;

Kaupp, M.; Marefat, A. K.; Khani, S. K.; Müller, T.; Mack, F.; Nguyen, B. D.; Parker, S. M.; Perlt, E.; Rappoport, D.; Reiter, K.; Roy, S. M. R.; Schmitz, G.; Sierka, M.; Tapavicza, E.; Tew, D. P.; Artur; Wullen, C. v.; Voora, V. K.; Weigend, F.; Wodynski, A.; Yu, J. M., TURBOMOLE: Modular program suite for ab initio quantum-chemical and condensed-matter simulations. *The Journal of Chemical Physics* **2020,** *152*, 184107-184107.

30.   Adamo, C.; Barone, V., Toward reliable density functional methods without adjustable parameters: The PBE0 model. *The Journal of Chemical Physics* **1999,** *110* (13), 6158-6170.

31.   Dunning, T. H., Gaussian basis sets for use in correlated molecular calculations. I. The atoms boron through neon and hydrogen. *Journal of Chemical Physics* **1989,** *90* (2), 1007-1023.

32.   Dennington, R.; Keith, T.; Millam, J., Gauss View, version 5. Semichem Inc.: Shawnee Mission, 2009.

33.   Petersson, G. A.; Al-Laham, M. A., A complete basis set model chemistry. II. Open‑shell systems and the total energies of the first‑row atoms. *Journal of Chemical Physics* **1991,** *94* (9), 6081-6090.